HHS Public Access

Author manuscript

Clin Sci (Lond). Author manuscript; available in PMC 2021 November 16.

Published in final edited form as:

Clin Sci (Lond). 2021 January 29; 135(2): 409–427. doi:10.1042/CS20201340.

Gastrin, via activation of PPARα, protects the kidney against hypertensive injury

Daqian Gu[1,2,*], **Dandong Fang**[1,2,*], **Mingming Zhang**[1,2], **Jingwen Guo**[1,2], **Hongmei Ren**[1,2], **Xinyue Li**[1,2], **Ziyue Zhang**[1,2], **Donghai Yang**[1,2], **Xue Zou**[1,2], **Yukai Liu**[1,2], **Wei Eric Wang**[1,2], **Gengze Wu**[1,2], **Pedro A. Jose**[3], **Yu Han**[1,2], **Chunyu Zeng**[1,2,4,5]

[1]Department of Cardiology, Daping Hospital, The Third Military Medical University, Chongqing, P.R. China

[2]Chongqing Key Laboratory for Hypertension Research, Chongqing Cardiovascular Clinical Research Center, Chongqing Institute of Cardiology, Chongqing, P.R. China

[3]Department of Medicine, Division of Renal Disease and Hypertension, and Department of Pharmacology and Physiology, The George Washington University School of Medicine and Health Sciences, Washington D.C., U.S.A.

[4]State Key Laboratory of Trauma, Burns and Combined Injury, Daping Hospital, The Third Military Medical University, Chongqing, P.R. China

[5]Cardiovascular Research Center of Chongqing College, Department of Cardiology of Chongqing General Hospital, University of Chinese Academy of Sciences, Chongqing, P.R. China

Abstract

Hypertensive nephropathy (HN) is a common cause of end-stage renal disease with renal fibrosis; chronic kidney disease is associated with elevated serum gastrin. However, the relationship between gastrin and renal fibrosis in HN is still unknown. We, now, report that mice with angiotensin II (Ang II)-induced HN had increased renal cholecystokinin receptor B (CCKBR) expression. Knockout of CCKBR in mice aggravated, while long-term subcutaneous infusion of gastrin ameliorated the renal injury and interstitial fibrosis in HN and unilateral ureteral obstruction (UUO). The protective effects of gastrin on renal fibrosis can be independent of its regulation of blood pressure, because in UUO, gastrin decreased renal fibrosis without

Correspondence: Chunyu Zeng (chunyuzeng01@163.com) or Yu Han (hanc2-823@126.com).
*These two authors contributed equally to this work.

CRediT Author Contribution

Daqian Gu: Data curation, Formal analysis, Methodology, Software, Writing — original draft. **Dandong Fang:** Data curation, Formal analysis, Methodology, Software. **Mingming Zhang:** Data curation, Formal analysis, Methodology. **Jingwen Guo:** Software. **Hongmei Ren:** Methodology. **Xinyue Li:** Methodology. **Ziyue Zhang:** Methodology. **Donghai Yang:** Supervision, Visualization. **Xue Zou:** Supervision. **Yukai Liu:** Supervision. **Wei Eric Wang:** Investigation, Supervision. **Gengze Wu:** Supervision. **Pedro A. Jose:** Funding acquisition, Resources, Writing — review & editing. **Yu Han:** Conceptualization, Methodology, Project administration, Writing — review & editing. **Chunyu Zeng:** Conceptualization, Funding acquisition, Resources, Writing — review & editing.

Competing Interests

The authors declare that there are no competing interests associated with the manuscript.

Human and Animal Rights

This study was conducted with the approval of the Institutional Animal Ethics Committee of The Third Military Medical University (Permit number: 2012[13]). All the animal studies were performed at the Animal Center of The Third Military Medical University.

affecting blood pressure. Gastrin treatment decreased Ang II-induced renal tubule cell apoptosis, reversed Ang II-mediated inhibition of macrophage efferocytosis, and reduced renal inflammation. A screening of the regulatory factors of efferocytosis showed involvement of peroxisome proliferator-activated receptor α (PPAR-α). Knockdown of PPAR-α by shRNA blocked the anti-fibrotic effect of gastrin *in vitro* in mouse renal proximal tubule cells and macrophages. Immunofluorescence microscopy, Western blotting, luciferase reporter, and Cut&tag-qPCR analyses showed that CCKBR may be a transcription factor of PPAR-α, because gastrin treatment induced CCKBR translocation from cytosol to nucleus, binding to the PPAR-α promoter region, and increasing PPAR-α gene transcription. In conclusion, gastrin protects against HN by normalizing blood pressure, decreasing renal tubule cell apoptosis, and increasing macrophage efferocytosis. Gastrin-mediated CCKBR nuclear translocation may make it act as a transcription factor of PPAR-α, which is a novel signaling pathway. Gastrin may be a new potential drug for HN therapy.

Introduction

Hypertensive nephropathy (HN) is a cause of chronic kidney disease (CKD), and is the second leading cause of end-stage renal disease, after diabetes nephropathy [1]. Fibrosis is one of the major pathological changes in HN, which is characterized by glomerular sclerosis, tubular atrophy, and interstitial fibrosis [2], consequently reducing renal function [3]. Although the exact mechanisms that lead to renal fibrosis are still not clear, there are some possible effective strategies to prevent or limit its progression [4-6]. Thus, a better understanding of the mechanisms involved in the progression of HN and finding appropriate methods to treat HN are essential.

Clinical data and animal experiments have shown that CKD is associated with increased serum gastrin levels [7,8]; there is an inverse relationship between glomerular filtration rate and serum gastrin levels. However, it is not clear if the increase in serum gastrin level with the decrease in glomerular filtration rate is the result of CKD or an attempt of the body to protect against kidney damage. Gastrin is produced by the G cells of the gastric antrum [9]. Among the different gut hormones, gastrin is the one that is taken up the most by renal proximal tubule (RPT) cells [10]. We have reported that the intrarenal infusion of gastrin induces natriuresis and diuresis in normotensive Wistar-Kyoto rats but not in spontaneously hypertensive rats [11]. However, a mixed meal increases serum gastrin to levels that are higher in hypertensive than normotensive humans [12]. Thus, we wondered whether gastrin has a beneficial effect in HN.

Many factors can impair renal function, such as hypertension, renal cell injury, inflammation, fibroblast formation, extracellular matrix accumulation, and epithelial–mesenchymal transition [1,13-15]. Among the different factors, inflammation plays a critical role in the development of HN [16]. Persistent inflammation can be the result of the generation of apoptotic cells and defective efferocytosis [17]. Gastrin can suppress or reverse cell apoptosis by activation of the PI3K-AKT and ERK1/2 pathways [18], which are critical in inducing efferocytosis [19]. However, the role of gastrin in these processes, and whether gastrin could influence the development of HN through these processes are unknown.

Since fibrosis is important in pathogenesis of HN [14,20], we treated mice with HN or unilateral ureteral obstruction (UUO) with gastrin and analysed the influence of gastrin on renal fibrosis. Due to the critical role of inflammation in the development of fibrosis in HN [14,20], we also tested the effects of gastrin on inflammation and fibrosis *in vitro* in RPT cells and monocytic RAW264.7 cells. The present study aimed to elucidate the relationship between gastrin and HN, as well as how gastrin influences HN.

Methods

Animals

Cholecystokinin receptor B (CCKBR)-deficient ($CCKBR^{-/-}$) mice [21] were obtained from Jackson Laboratory and bred in an AAALAC-accredited facility. The wild-type (WT, $CCKBR^{+/+}$) mice housed in the same cages were used as control. The mice were housed in a controlled environment (20 ± 2°C, 12/12 h light/dark cycles), with free access to water and standard rodent chow. All experimental procedures were approved by the Animal Care and Use Committee of The Third Military Medical University. All experiments conformed to the guidelines for the ethical use of animals, and all efforts were made to minimize animal suffering and reduce the number of animals used. All the *in vivo* studies were performed at the Animal Center of The Third Military Medical University.

HN model

WT ($CCKBR^{+/+}$) and $CCKBR^{-/-}$ mice (8 weeks old) were used in these experiments. Alzet osmotic minipumps (Model 1004, Durect Corporation, CA) were subcutaneously implanted in the dorsal region of the body under isoflurane anesthesia. The minipumps were loaded with saline as vehicle alone (control) or chemicals and infused at a rate of 2.64 μl/days (d) for 28 d as described previously [22]. The infusate contained the saline vehicle (control, 2.64 μl/d, 100 μl in the pump), angiotensin II (Ang II, 1.44 mg/kg body weight/d, 100 μl in the pump, Sigma-Aldrich, Shanghai, China) or/and gastrin (120 μg/kg body weight/d, 100 μl in the pump, Sigma-Aldrich) [23,24]. Blood pressure was measured weekly by an investigator who was blinded to the group information, using the tail-cuff method. (ML125, PowerLab, AD Instruments, Castle Hill, Australia). After 28 d of treatment, the mice were weighed, serum and urine were collected (blood was collected from the eyes), and then the mice were killed with an overdose of 6% chloral hydrate (6 ml/kg). The kidneys were immediately excised, weighed, and processed for analysis.

UUO model

UUO was performed, using an established protocol [25]. Briefly, the WT ($CCKBR^{+/+}$) mice (8 weeks old) were anesthetized followed by a lateral incision at the back. After the left ureter was exposed, it was tied with a silk suture at two points and permanently ligated. Saline, as vehicle (control, 2.64 μl/d, 100 μl in the pump), or gastrin (120 μg/kg body weight/d, 100 μl in the pump) was infused subcutaneously, via Alzet osmotic minipumps, as described above. After 7 d, the mice were weighed, serum and urine were collected (blood was collected from the eyes), and then the mice were killed with an overdose of 6% chloral hydrate (6 ml/kg). The kidneys were immediately excised, weighed, and processed for analysis.

Cell culture and RNA interference

RAW264.7 cells (ATCC®-TIB-71™) and primary macrophages were maintained in RPMI164. Mouse RPT cells used in these experiments were originally provided by Dr Ulrich Hopfer of the Case Western Reserve University School of Medicine [26,27] and maintained in DMEM-F-12 with 10% fetal bovine serum, 100 IU/ml penicillin, 100 IU/ml streptomycin, and 250 g/ml amphotericin B. The cells were grown at 37°C and 5% CO_2 in humidified air. In the apoptosis experiments, the RPT cells were treated with Ang II (10^{-8} mol/l) [28], gastrin (10^{-7} mol/l) [11], or CI988 (CCKBR inhibitor, 10^{-7} mol/l) [29] for 48 h. In the efferocytosis experiments, RAW264.7 cells were treated with Ang II (10^{-8} mol/l), gastrin (10^{-7} mol/l), and CI988 (10^{-7} mol/l) for 24 h. The vehicle groups were treatedwith the same volume of saline, instead of the drugs. The silencing of peroxisome proliferators activated receptor α (PPAR-α) was performed by PPARα-specific shRNA transfected with lentiviral particles (lenti-shPPAR-α, Santa Cruz, Shanghai, China). Scramble shRNA transfected with lentiviral particles (Santa Cruz) was used as the control oligonucleotide. In these *in vitro* experiments, the cells were collected 3 d after transfection to determine the efficiency of gene knockdown using qRT-PCR.

Urine and blood analyses

At the end of the experiments, urine was collected for 24 h in mice placed individually in metabolic cages. Serum creatinine was determined using a Hitachi multi-analyzer (Hitachi, 205D; Hitachinaka, Japan). The concentrations of urinary albumin were measured by the Coomassie brilliant blue G250 method, using bovine serum albumin as standard. Briefly, 10 μl of urine were denatured with loading buffer and then resolved by electrophoresis on an 8% sodium dodecyl sulfate polyacrylamide gel. The proteins on the gel were detected by Coomassie blue staining.

Renal histopathology

The kidneys were fixed and then dehydrated in increasing concentrations of ethanol. Then, the treated kidneys were cleared in xylene and embedded in paraffin. The samples were cut into 4 μm thick sections for staining, followed by staining with hematoxylin and eosin; morphology was scored to determine the extent of renal damage. These histopathologic damages included tubule epithelial cell swelling and vacuolization, cast formation, and desquamation. Scoring was: 0, normal; 1, ≤10% injury; 2, 11–25% injury; 3, 26–50% injury; 4, 51–75%, and 5, >75% injury, modified from Gao et al. [30] Tubular atrophy was assessed by staining the renal sections with periodic acid–Schiff (PAS), and tubular atrophy was defined as loss of tubular nuclei, reduced tubular diameter, and thickened tubular basement membrane. The tubular atrophy index was quantified by measuring the ratio of the number of dead tubule cells to the number of total tubule cells. Renal fibrosis was assessed by staining the renal sections with Masson's trichrome and Sirius Red. The glomerular collagen content was quantified by measuring the ratio of fibrosis staining area to the total staining area (examined under a microscope). To quantify the number of glomeruli (per area, 10×), 20 serial sections of the entire kidney were used (per animal, n=3) [31]. Quantification was conducted by an investigator who was blinded to the group information of the samples.

TUNEL assay

Apoptosis was detected by TUNEL assay (Roche, Shanghai, China). In brief, the kidney sections were placed on slides heated at 65°C, washed in xylene, and dehydrated through a graded series of ethanol solutions. Then, the sections were incubated in 10 μg/ml protease K (Sigma-Aldrich) for 30 min at 37°C, followed with 0.5% Triton X-100 for 10 min. The sections were rinsed with PBS (5 min, three times), and then incubated in 50 μl of TUNEL reaction mixture for 60 min at 37°C, in a humidified atmosphere in the absence of light. After washing with PBS (5 min, three times), the sections were stained with DAPI, before being imaged under a laser scanning confocal microscope. The number of TUNEL-positive nuclei was quantified in 10 high-power fields from three different sections. Data were expressed as the average number of TUNEL-positive nuclei per high-power field. Quantification was conducted by an investigator who was blinded to the group information of the samples.

Immunofluorescence microscopy

The kidney sections in glass slides were deparaffinized and rehydrated. Antigen was retrieved by heating in microwave the kidney sections in sodium citrate-EDTA antigen retrieval solution. The cells fixed on glass slides were treated with 4% paraformaldehyde. After PBS rinses (5 min, three times), the kidney sections and cells were mixed with immunostaining blocking solution for 1 h at room temperature to prevent nonspecific antibody binding. Then, the kidney sections and cells were incubated with the primary antibody at 4°C overnight. After washing with PBS for 5 min, three times, the sections and cells were incubated with secondary antibody at room temperature for 1 h. Finally, after washing with PBS (5 min, three times), the sections and cells were stained with DAPI before being imaged under a laser scanning confocal microscope. The following antibodies used were: F4/80, CDH16, cleaved caspase 3, CCKBR, goat anti-mouse IgG (FITC), goat anti-rabbit IgG (Cy3), goat anti-mouse IgG (Cy3), donkey anti-goat IgG (Alexa Fluor™ Plus 647), and donkey anti-goat IgG (Cy3). The information on these antibodies is listed in Supplementary Table S1. The images were collected by an investigator who was blinded to the group information of the samples.

Preparation of peritoneal macrophages

The WT ($CCKBR^{+/+}$) and $CCKBR^{-/-}$ mice were intraperitoneally injected with 1 ml of 4% thioglycollate broth (Sigma-Aldrich) at 0 d. Four days later, the mice were killed [32]. The abdomen was opened, leaving the peritoneum intact. The peritoneal cavity was quickly flushed with 10 ml of wash buffer (RPMI1640, 2% FBS, 0.04% EDTA), using a 10 ml syringe attached to an 18 G needle. The wash buffer was retrieved slowly with the same needle/syringe, into a 50 ml tube. Peritoneal lavage was performed twice with 1 × PBS and the peritoneal macrophages were suspended in RPMI1640 tissue culture medium at a density of 2×10^6 cells/ml. An aliquot of 500 μl was placed into each well of a 24-well plate. The plates with the cells were incubated in a tissue culture incubator for 2 h at 37°C. The floating cells were aspirated into 500 μl of fresh culture medium, twice [33].

Preparation of kidney-resident macrophages

The renal macrophages from mouse kidneys were isolated, as previously described [34]. In brief, kidneys from WT ($CCKBR^{+/+}$) mice were finely minced and digested with 0.4 mg/ml collagenase D and 0.01 mg/ml DNAse I in DMEM, supplemented with 10% heat-inactivated fetal calf serum for 45 min at 37°C. The cell suspensions were sequentially filtered through 75 and 40 μm nylon meshes and were washed with HBSS, without Ca^{2+} and Mg^{2+} (Invitrogen, U.S.A.). Single-cell suspensions were separated, using Percoll density gradient (70% and 40%) centrifugation. The macrophage-enriched cell suspension was aspirated from the Percoll interface. Then, $F4/80^{+}$ cells were isolated from the cell suspension using anti-F4/80 MicroBeads UltraPure (Miltenyi Biotec Technology, Shanghai, China). The isolated macrophages were stained with anti-F4/80 and CD11b and were assessed by flow cytometry. This method yielded greater than 90% macrophages.

In vivo efferocytosis analysis

For *in vivo* peritoneal macrophage phagocytosis (efferocytosis) assays, $CCKBR^{-/-}$ or WT ($CCKBR^{+/+}$) mice were subcutaneously infused, via an Alzet osmotic minipumps, with the saline vehicle (control, 2.64 μl/d), Ang II (1.44 mg/kg body weight/d), and/or gastrin (120 μg/kg body weight/d) for 28 d. Subsequently, peritonitis was induced in these mice by the intraperitoneal injection of 1 ml of 4% thioglycollate broth [32]. Three days after the injection, 1×10^7 (1 ml) BCECF AM-labeled apoptotic Jurkat cells were intraperitoneally injected into these mice [35]. The mice were killed after 1 h, and peritoneal lavage was performed with 5 ml ice-cold PBS that were subsequently transferred into plastic tubes, as described above. The cells were washed twice, and a single-cell suspension of peritoneal flush was stained with anti-F4/80 and CD11b to identify the macrophages. The cells were analysed by flow cytometry, and the number of peritoneal macrophages ingesting apoptotic thymocytes was counted [35]. The information on the above antibodies is listed in Supplementary Table S1.

In vitro efferocytosis analysis

Before the induction of apoptosis, Jurkat cells were stained with BCECF AM (Beyotime, Shanghai, China), and rinsed with 1 × PBS, and then incubated for 30 min at room temperature. Apoptosis was induced by irradiating the Jurkat cells under a UV (254 nm) lamp for 30 min, followed by incubation under normal cell culture conditions for 2–3 h [36]. This method routinely yielded greater than 80% apoptotic cells. RAW264.7 cells (1×10^5 cells/well) were stained with Dil (Beyotime) and plated in 12-well plates. After 24-h treatment with saline vehicle (control, 20 μl), gastrin (10^{-7} mol/l) [11], Ang II (10^{-8} mol/l) [28], or the CCKBR inhibitor, CI988 (10^{-7} mol/l) [29], the cells were exposed to BCECF AM-labeled apoptotic Jurkat cells (1×10^6 cells/well) for 1 h. Undigested cells were removed by washing three times with ice-cold PBS and efferocytosis of apoptotic cells was visualized using fluorescence microscopy. Peritoneal macrophages were treated the same way. The phagocytosis index was expressed as the percentage of macrophages binding or containing at least one ingested Jurkat cells [37]. Kidney-resident macrophages treated with gastrin (10^{-7} mol/l) and lenti-sh-PPAR-α were also used for efferocytosis analysis.

Subcellular fractionation

RPT and RAW264.7 cells were plated in cell culture dish for 24 h, and then treated with gastrin (10^{-7} mol/l) for 0, 5, 15, 30 min, 1, and 24 h. Then, the cells were washed two times with cold PBS, lysed in 1 ml of cytoplasmic lysis buffer (10 mM MES, pH 6.2, 10 mM NaCl, 1.5 mM $MgCl_2$, 1 mM EDTA, 5 mM DTT, 1% Triton X-100, 1 mM AEBSF, and 1 mM NaF) for 10 min on ice, scraped into Eppendorf tubes, and centrifuged for 10 min at 3000 rpm in a bench-top centrifuge. The supernatant was recentrifuged at 13,000 rpm for 20 min, and supernatant collected, as the cytoplasmic fraction. The pellet from the first centrifugation was washed three times with 1 ml of cytoplasmic lysis buffer, supplemented with 1% NP-40 and once with cytoplasmic lysis buffer, without addition of detergents. The purified nuclear pellet was resuspended in 0.5 ml of nuclear extraction buffer (25 mM Tris-HCl, pH 10.5, 1 mM EDTA, 0.5 M NaCl, 5 mM β-mercaptoethanol, and 0.5% Triton X-100), vortexed for 10 min at 4°C, and centrifuged for 20 min at 13,000 rpm; the supernatant was collected as the nuclear fraction [38]. The renal tissues from the different groups of mice were fractionated into nuclear and cytoplasmic components, as above.

Immunoblotting

The kidney tissues were lysed in RIPA buffer, supplemented with protease inhibitors, and denatured with loading buffer. The nuclear and cytoplasmic fractions were also denatured with loading buffer. The protein samples were collected and stored at −20°C, until use. The protein samples were separated by SDS-PAGE with 10–15% polyacrylamide gel and then electroblotted onto nitrocellulose membranes (Amersham Life Science, Arlington, TX). The blots were blocked in Tris-buffered saline containing 5% nonfat dry milk for 1 h at room temperature with constant shaking and then incubated with primary antibodies (TNF-α, IL-6, IL-1β, cleaved caspase 3, CCKBR, GAPDH, PCNA), overnight at 4°C. The secondary antibodies (Goat anti-Rabbit IR Dye 800, Donkey anti-Goat IR Dye 800, Goat anti-Mouse IR Dye 800) were used to bind their respective primary antibody at room temperature for 1 h. The bound complexes were detected using the Odyssey Infrared Imaging System (Li-Cor Biosciences). The images were analysed through the Odyssey Application Software to obtain the integrated intensities. The information on the above antibodies is listed in Supplementary Table S1. Then original images are in Supplementary Figure S7.

Reverse transcription-PCR

The cells were treated with the saline vehicle (control, 25 μl), gastrin (10^{-7} mol/l), and/or CI988 (10^{-7} mol/l) for 24 h. Total RNA from tissues and cells was isolated using a Trizol procedure (Invitrogen). Two micrograms of total RNA were used to synthesize cDNA, which served as the template for the amplification of different genes. The primers used to measure the gene expression are listed in Supplementary Table S2. The amplification was performed under the following conditions: 94°C for 2 min, followed by 35 cycles of denaturation at 94°C for 30 s, annealing at 58°C for 30 s, and extension at 72°C for 45 s. This was followed by a final extension at 72°C for 10 min.

Transfection and luciferase reporter assay

PPAR-α promoter activity was measured, as previously described [39]. HEK293 cells were plated at a density of 1×10^5 cells/well in 24-well plates for 24 h and then transfected with different plasmids, using Lipofectamine 2000 (Invitrogen), following the manufacturer's instructions. The cells were co-transfected with CCKBR-FLAG, PPAR-α promoter-pGL3, and pRL-TK (a Renilla luciferase reporter vector is the internal control). One day after transfection, the cells were serum-starved and incubated in serum-free media. Then, the cells were treated with gastrin (10^{-7} mol/l) or saline vehicle (control, 10 µl) for 24 h. The transfected cells were assayed for Firefly and Renilla luciferase activities in a luminometer by the Dual-Luciferase Reporter Assay System (Beyotime), according to the manufacturer's instructions. The luciferase readings of each sample were normalized against the pRL-TK levels, and the relative light unit intensity was calculated as the ratio of firefly luciferase to Renilla luciferase. All experiments were performed in triplicate and repeated at least three times.

Cut&tag assay

The Cut&tag is a new method to extract the DNA bound to protein [40], CCKBR protein, in this instance. RPT and RAW264.7 cells were treated with saline vehicle (control, 25 µl) or gastrin (10^{-7} mol/l) for 1 h in six-well plates. Then, the cells were harvested and treated according to the manufacturer's instructions. The DNAs were extracted and subjected to PCR. The information on the mouse PPAR-α promoter primers is listed in Supplementary Table S2.

A detailed, step-by-step protocol can be found at: https://www.novoprotein.com.cn/Public/Uploads/uploadfile/files/20191126/20191126132754_5ddcb7da4dd15.pdf.

Nuclear localization signal (NLS) motif and DNA-binding domain analysis

NLS motif prediction is based on NLStradamus (http://www.moseslab.csb.utoronto.ca/NLStradamus/) and DNA binding domain analysis is based on Predictprotein (https://www.predictprotein.org/home) [41].

Statistical analysis

All data are expressed as mean ± SD, unless otherwise stated. GraphPad-Prism 6.0 and SPSS 17.0 were used to perform the statistical analysis. Student's unpaired *t*-test was used to compare two independent groups. In experiments comparing multiple time points, separate t-tests were used for each time point. For a comparison of ≥3 groups, one-way ANOVA was used and Tukey as post-hoc test. All tests were two-tailed with a significant difference set at $P < 0.05$. Survival rates were compared using the log-rank test.

Results

CCKBR deficiency aggravates Ang II-induced renal injury

The WT ($CCKBR^{+/+}$) mice infused with Ang II (1.44 mg/kg body weight/d x 28 d) had increased serum creatinine and urinary albumin, in agreement with previous reports [23,42]. The increase in serum creatinine and urinary albumin (Figure 1A,B, Supplementary Figure

S1A and 1B, performed independently of each other) were accompanied by increased renal injury and fibrosis (Supplementary Figure S1C and 1D), as well as increased renal mRNA and protein expressions of CCKBR compared with the vehicle-treated group (Supplementary Figure S1E-G).

To investigate the role of CCKBR in Ang II-induced renal injury, similar studies were performed in $CCKBR^{-/-}$ mice. $CCKBR^{-/-}$ mice had normal serum creatinine and urinary albumin at baseline (Figure 1A,B). However, after 28 d of Ang II infusion, serum creatinine (Figure 1A) and urinary albumin (Figure 1B and Supplementary Figure S2A) increased to a much greater extent in $CCKBR^{-/-}$ than WT ($CCKBR^{+/+}$) mice. In addition, the blood pressure was significantly higher in $CCKBR^{-/-}$ than WT ($CCKBR^{+/+}$) mice (Supplementary Figure S2B). The median survival time was reduced by about 30% in $CCKBR^{-/-}$ mice (Figure 1C). These results suggest that CCKBR deficiency aggravates Ang II-induced renal injury.

Consistent with the greater impairment of renal function in $CCKBR^{-/-}$ than WT ($CCKBR^{+/+}$) mice infused with Ang II, pathological changes were worse in $CCKBR^{-/-}$ than WT ($CCKBR^{+/+}$) mice. Lack of CCKBR, per se, did not increase renal tubular dilatation, tubular atrophy, tubular fibrosis, interstitial fibrosis (Figure 1D-F), or expression of fibrosis-related genes (Figure 1G-I) but these variables were markedly increased by the 28-d infusion of Ang II, especially in $CCKBR^{-/-}$ mice. The pathological changes were mainly related to tubular injury, because Ang II infusion did not alter the number of glomeruli (Supplementary Figure S2C), although there was glomerular injury, evidenced by the increase in serum creatinine and urinary albumin (Supplementary Figure S1 A and 1B) and glomerular sclerosis (Supplementary Figure S2C).

Gastrin, independent of blood pressure, attenuates Ang II-induced renal injury

Since the germline deletion of CCKBR aggravated the Ang II-induced renal damage, we wondered whether gastrin, a CCKBR agonist, could alleviate the renal injury in Ang II-treated WT ($CCKBR^{+/+}$) mice. Under isoflurane anesthesia, an osmotic minipump filled with gastrin was subcutaneously implanted in the dorsal region of the body, so that gastrin (120 μg/kg body weight/d) can be infused subcutaneously for 4 weeks in WT ($CCKBR^{+/+}$) mice. Gastrin, per se, had no effect on serum creatinine and urinary albumin. However, gastrin ameliorated the increased serum creatinine (Figure 2A) and urinary albumin (Figure 2B) in the Ang II-treated WT ($CCKBR^{+/+}$) mice. Gastrin also minimized the Ang-II-mediated pathological injury (Figure 2C-E) and the increased expression of fibrosis-related genes (Figure 2F-H). In addition, we found that CCKBR knockout prevented the beneficial effects of gastrin on Ang-II-induced renal injury *in vivo* (Supplementary Figure S3A-C).

We also noticed that gastrin minimized the increase in blood pressure caused by the 28-d infusion of Ang II (Supplementary Figure S4A). To determine if the protective effect of gastrin on renal function and pathology was dependent on its blood pressure lowering effect, we also studied the UUO model. The UUO model does not affect blood pressure; its main feature is renal fibrosis [43,44], which is also thought to be the major renal pathologic change of HN [45,46]. Thus, we treated the UUO mice with the osmotic minipump infused with gastrin (120 μg/kg body weight/d) for 7 d (Supplementary Figure S4B).

Gastrin treatment had no effect on the blood pressure of the UUO mice, which is normal (Supplementary Figure S4C), but it reduced the renal injury and fibrosis (Figure 3A-C) and expression of fibrosis-related genes (Figure 3D-F). These results demonstrated that gastrin can exert its renal-protective effects via both hemodynamic and non-hemodynamic mechanisms.

Gastrin plays a protective effect in HN by increasing macrophage efferocytosis and reducing RPT cell apoptosis

Since inflammation plays an important role in the progression of HN [16], we, next, tested the levels of inflammation in the different groups. We found that CCKBR deficiency significantly increased the macrophage infiltration of the kidney induced by Ang II, but gastrin treatment reversed the effect of Ang II (Figure 4A). Compared with Ang II-treated WT ($CCKBR^{+/+}$) mice, Ang II-treated $CCKBR^{-/-}$ mice showed a greater increase in the renal levels of inflammation-related genes (mRNA and protein), but gastrin treatment almost normalized the effect of Ang II in WT ($CCKBR^{+/+}$) mice (Figure 4B-H), suggesting that gastrin may protect against HN by decreasing inflammation.

Although the pathogenesis of the inflammation in HN is not exactly known, an increase in tubule cell apoptosis and decrease in macrophage efferocytosis may augment the inflammation [14,47,48]. Ang II increased the quantity of TUNEL-positive nuclei in WT ($CCKBR^{+/+}$) mice but to a greater extent in $CCKBR^{-/-}$ mice. By contrast, gastrin had no effect on TUNEL staining in saline vehicle-treated WT ($CCKBR^{+/+}$) mice but ameliorated the increase in TUNEL-positive cells induced by Ang II (Figure 5A). The amount of cleaved caspase 3, the activated form of caspase 3, a marker of apoptosis [49], was not affected by germline deletion of CCKBR or gastrin infusion. However, cleaved caspase 3 protein was increased by Ang II to a greater extent in $CCKBR^{-/-}$ than WT ($CCKBR^{+/+}$) mice; gastrin infusion almost normalized the effect of Ang II in WT ($CCKBR^{-/-}$) mice (Figure 5B,C).

The phagocytosis of apoptotic cells by peritoneal macrophages (efferocytosis) was decreased in saline vehicle-treated $CCKBR^{-/-}$ mice but increased in gastrin-treated WT ($CCKBR^{+/+}$) mice to a greater extent than in saline vehicle-treated WT ($CCKBR^{+/+}$) mice. Ang II decreased the efferocytosis in WT ($CCKBR^{+/+}$) mice, and CCKBR deficiency augmented it. However, gastrin increased the efferocytosis in Ang II-treated WT ($CCKBR^{+/+}$) mice to the levels seen in saline vehicle-treated (control) mice (Figure 5D and Supplementary Figure S5A).

Because the beneficial effect of gastrin on macrophage efferocytosis and RPT cell apoptosis occurred simultaneously *in vivo*, we wanted to look further into this relationship in *in vitro* studies. We treated RPT cells and RAW264.7 cells with Ang II (10^{-8} mol/l) [28] or gastrin (10^{-7} mol/l) [11] for 24 h. Our results showed that the Ang II-induced RPT cell apoptosis, determined by the increased expression of cleaved caspase 3, was reduced to normal by gastrin (Figure 5E), indicating that gastrin has direct protective effect on RPT cell apoptosis, independently of its effect on macrophage efferocytosis. Nevertheless, the inhibition of Ang II on efferocytosis in RAW264.7 cells was also reversed by gastrin (Figure 5F). In addition, we found that the mRNA expression of efferocytosis markers, such as C1qa, C1qb, CD36, GAS6, and MERTK, but not MFGE8 [35] were increased by gastrin (Supplementary Figure

S5B). The specificity of gastrin on the CCKBR was determined by using the CCKBR inhibitor, CI988 (10^{-7} mol/l) [29]; CI988 prevented the stimulatory effect of gastrin on efferocytosis in RAW264.7 cells (Figure 5F). Similarly, in peritoneal macrophages from CCKBR$^{-/-}$, the ability of gastrin to block the inhibitory effect of Ang II on efferocytosis was also lost, confirming that gastrin exerts its protective effects, via CCKBR (Figure 5G).

Role of PPAR-α in the gastrin-mediated protective effects on Ang II-induced renal injury

Because the transcription factors PPAR-δ, PPAR-γ, HO-1, and LXR have been shown to regulate efferocytosis [35,50], we determined if they were involved in the protective effects of gastrin. PPAR-α can increase gastrin expression in G-cells [51]. We found that gastrin treatment up-regulated the mRNA expression of PPAR-α, but not PPAR-δ, PPAR-γ, HO-1, LXR-α, or LXR-β in RAW264.7 and RPT cells (Figure 6A and Supplementary Figure S6A). Moreover, the increase in the expression of PPAR-α induced by gastrin in macrophages and RPT cells was prevented when the CCKBR was blocked by the CCKBR antagonist CI988 or when the CCKBR receptor was germline-deleted, as in CCKBR$^{-/-}$ mice, indicating that gastrin, via CCKBR, regulates PPAR-α expression (Figures 6B-D). Similar effects on PPAR-α expression were found in renal tissues and renal tissue-resident macrophages (Supplementary Figure S6B-D). The critical role of PPAR-α in gastrin-mediated efferocytosis and anti-apoptosis was further investigated by using shRNA (silencing efficiency in Supplementary Figure S6E and F). After down-regulation of PPAR-α expression by shRNA, the protective effects of gastrin on macrophage phagocytosis (efferocytosis) (Figure 6E,F and Supplementary Figure S6G) and RPT cell apoptosis (Figure 6G) were lost.

A previous study showed that CCKBR is expressed not only on the cell membrane, but also in the cytoplasm and nucleus [52]. Through bioinformatics analysis, we found that CCKBR contains two potential NLS motifs and two DNA binding domains (Figure 7A,B). Therefore, we wondered whether CCKBR can translocate from the cytosol into the nucleus to induce PPAR-α expression. First, we found that incubation of RAW264.7 and RPT cells with gastrin increased CCKBR translocation from cytosol to nucleus, determined by western blot and immunofluorescence analyses, and the translocation occurred as early as 5 min, with the peak detected at about 15–30 min (Figure 7C,D). To determine whether CCKBR forms a complex with the PPAR-α promoter, we performed a Cut&tag assay in RAW264.7 and RPT cells treated with gastrin or saline vehicle (control). Cut&tag-qPCR analysis showed a significant increase in the binding of CCKBR to the PPAR-α promoter region in cells treated with gastrin (Figure 7E,F). To examine further the effect of CCKBR on the transcriptional activity of PPAR-α, we performed a luciferase reporter assay in HEK293 cells heterologously expressing CCKBR-FLAG, PPAR-α promoter-pGL3, and pRL-TK (a Renilla luciferase reporter vector as internal control). Our results showed that the PPAR-α promoter activity was up-regulated by gastrin (10^{-7} mol/l) treatment of the HEK293 cells (Figure 7G). These results indicated that CCKBR can bind to the promoter region of PPAR-α and increase PPAR-α gene transcription ability.

Discussion

"Gastrointestinal-kidney axis" has attracted increasing attention because its role in fluid and electrolyte balance and blood pressure regulation [53-55]. The role of the gastrointestinal tract in the maintenance of normal homeostasis by the kidney has been demonstrated in many studies [56-58]. However, most of these studies focused on the effect of the gut microbiota. The effects of gut hormones and receptors on renal diseases are still poorly understood. Glucagon-like peptide1 (GLP-1), ghrelin, cholecystokinin, and gastrin are components of the "Gastrointestinal-kidney axis" [53-55]. Among them, GLP-1 plays a critical role in ameliorating diabetic nephropathy by decreasing oxidative stress and improving metabolic anomalies [59,60]. Ghrelin mitigates renal damage induced by ischemia-reperfusion and Ang II [61,62], and cholecystokinin protects against diabetic kidney injury by suppressing the activation of macrophages and expression of pro-inflammatory genes [63]. Gastrin is one of the gut hormones and is the major gastrointestinal hormone taken up by RPT cells [10]. Our previous studies showed that gastrin interacts with D_1 and D_5 dopamine receptors to regulate natriuresis and diuresis [11,64]. In addition, gastrin can stimulate renal dopamine production and decrease Na^+,K^+-ATPase activity in RPT cells [65,66]. However, there are few studies about the influence of gastrin in renal diseases. In this study, we showed that gastrin can ameliorate the renal functional and morphologic abnormalities caused by HN and UUO.

A prominent pathological feature in hypertensive kidney disease is inflammation, tubular atrophy, and renal fibrosis [2]. The degree of renal fibrosis correlates with the prognosis of CKD [67]. However, the underlying mechanisms involved in Ang II-induced hypertensive renal fibrosis are incompletely understood. Recent studies have shown that Ang II can induce apoptosis and inflammatory cell infiltration (such as T cells and macrophages) of renal cells/kidney [46,68,69], which could lead to irreversible fibrosis [2]. Since cell death and effective clearance of dying cells are fundamental processes that maintain homeostasis, it is possible that the infiltrating macrophages participate in the efferocytosis of dying renal tubule cells [47]. It has been reported that Ang II impairs macrophage efferocytosis [37]. Thus, in the microenvironment of the hypertensive kidney, Ang II-induced excessive cell death and defective efferocytosis may account for the persistence of inflammation [70-72]. However, the contribution of tubular cell death and efferocytosis on the inflammation is still unknown in HN. In our current study, we found that Ang II induced obvious tubule cell apoptosis and defective efferocytosis both *in vitro* and *in vivo*. CCKBR deficiency aggravated the above phenotypes in HN. We wondered whether decreasing cell death and increasing efferocytosis could have therapeutic effects. In our experiments, gastrin treatment significantly decreased the apoptosis of renal tubule cells and increased the efferocytosis by macrophages in HN. These results were also found in RPT cells and RAW264.7 cells, which may explain the resolution of the inflammation in HN treated with gastrin.

In this study, we demonstrated that the renoprotective effects of gastrin were related to the transcription of PPAR-α. Activation of PPAR-α has been proved to be renoprotective in previous reports [73,74]. Previous studies have also demonstrated that PPAR-α plays a key role in attenuating fibrosis in different animal models of renal fibrosis, such as remnant kidney model, diabetic renal fibrosis, and lipotoxicity-induced renal fibrosis [75-77].

Moreover, the reported protective role of PPAR-α in UUO and HN [5,78] is consistent with our present study. We found that gastrin can protect RPT cells from Ang II-induced apoptosis partly through PPAR-α, similar to the reported anti-apoptotic effects of PPAR-α [79]. However, the current studies show for the first time a role of PPAR-α in efferocytosis. We found that gastrin-induced efferocytosis is strongly associated with the transcription of PPAR-α. This may be related to the ability of PPAR-α to regulate the expression of efferocytosis-related genes. In our experiments, the stimulatory effect of gastrin on the mRNA expression of C1qa, C1qb, CD36, GAS6 can be inhibited by silencing PPAR-α. It is interesting that gastrin, as a sensor for eating [51,80,81], can also regulate the feeding of macrophages, hinting that it might be a critical bond between “people eating” and “cell eating”.

Some studies have shown that some membrane receptors, such as the insulin receptor and epidermal growth factor receptor, can enter the nucleus to participate in transcriptional regulation [82,83]. Similarly, we found that CCKBR can translocate into the nucleus to regulate PPAR-α mRNA expression. Moreover, we found that CCKBR contains potential NLS motifs and DNA binding domains, according to bioinformatics analysis, similar to the insulin receptor and epidermal growth factor receptor [84,85]. In addition, the epidermal growth factor receptor has been demonstrated to be a transcription factor, and insulin receptor can bind with Host Cell Factor C1 and other transcription factors to regulate gene expression [82,83]. CCKBR can also translocate or be translocated into the nucleus and act like a transcription factor. In the present study, we only demonstrated that CCKBR can form a complex with the PPAR-α promoter and enhance the PPAR-α promoter activity. Whether or not CCKBR can work as a transcription factor is still unknown. How nuclear CCKBR regulates genes requires further investigations.

In summary, CCKBR plays a protective role in the kidney against hypertension-mediated injury. PPAR-α is critical in signaling the gastrin-mediated protection by reducing renal tubule cell apoptosis and enhancing macrophage-mediated efferocytosis, thus, alleviating renal inflammation and ameliorating renal injury and fibrosis in HN. Our present study suggests that gastrin might be a potential therapy option for HN.

Supplementary Material

Refer to Web version on PubMed Central for supplementary material.

Funding

These studies were supported in part by grants from the National Key R&D Program of China [grant number 2018YFC1312700]; National Natural Science Foundation of China [grant numbers 31430043 and 81930008]; Program of Innovative Research Team by National Natural Science Foundation [grant number 81721001]; Clinical Medical Research Personnel Training Program of the Army Medical University [grant number 2018XLC10I2]; and National Institutes of Health (USA) [grant numbers R01DK039308, R01DK119652, and P01HL074940].

Data Availability

The data and the access links underlying this article are available in the article and in its online Supplementary Material.

Abbreviations

Ang II	angiotensin II
CCKBR	cholecystokinin receptor B
CKD	chronic kidney disease
GLP-1	glucagon-like peptide-1
HN	hypertensive nephropathy
NLS	nuclear localization signal
PPAR-α	peroxisome proliferator-activated receptor α
UUO	unilateral ureteral obstruction
WT	wild-type

References

1. Seccia TM, Caroccia B and Calo LA (2017) Hypertensive nephropathy. Moving from classic to emerging pathogenetic mechanisms. J. Hypertens 35, 205–212, 10.1097/HJH.0000000000001170 [PubMed: 27782909]
2. Meguid El Nahas A and Bello AK (2005) Chronic kidney disease: the global challenge. Lancet 365, 331–340, 10.1016/S0140-6736(05)17789-7 [PubMed: 15664230]
3. Sun YB, Qu X, Caruana G and Li J (2016) The origin of renal fibroblasts/myofibroblasts and the signals that trigger fibrosis. Differentiation 92, 102–107, 10.1016/j.diff.2016.05.008 [PubMed: 27262400]
4. Kawai T, Masaki T, Doi S, Arakawa T, Yokoyama Y, Doi T et al. (2009) PPAR-gamma agonist attenuates renal interstitial fibrosis and inflammation through reduction of TGF-beta. Lab. Invest 89, 47–58, 10.1038/labinvest.2008.104 [PubMed: 19002105]
5. Li S, Mariappan N, Megyesi J, Shank B, Kannan K, Theus S et al. (2013) Proximal tubule PPARalpha attenuates renal fibrosis and inflammation caused by unilateral ureteral obstruction. Am. J. Physiol. Renal. Physiol 305, F618–627, 10.1152/ajprenal.00309.2013 [PubMed: 23804447]
6. Jung KJ, Kim J, Park YK, Yoon YR. and Park KM (2010) Wen-pi-tang-Hab-Wu-ling-san reduces ureteral obstructive renal fibrosis by the reduction of oxidative stress, inflammation, and TGF-beta/Smad2/3 signaling. Food Chem. Toxicol 48, 522–529, 10.1016/j.fct.2009.11.006 [PubMed: 19913069]
7. Hallgren R, Karlsson FA and Lundqvist G (1978) Serum level of immunoreactive gastrin: influence of kidney function. Gut 19, 207–213, 10.1136/gut.19.3.207 [PubMed: 344160]
8. McLeland SM, Lunn KF, Duncan CG, Refsal KR and Quimby JM (2014) Relationship among serum creatinine, serum gastrin, calcium-phosphorus product, and uremic gastropathy in cats with chronic kidney disease. J. Vet. Intern. Med 28, 827–837, 10.1111/jvim.12342 [PubMed: 24628683]
9. Michell AR, Debnam ES and Unwin RJ (2008) Regulation of renal function by the gastrointestinal tract: potential role of gut-derived peptides and hormones. Annu. Rev. Physiol 70, 379–403, 10.1146/annurev.physiol.69.040705.141330 [PubMed: 17988205]
10. Melis M, Krenning EP, Bernard BF, de Visser M, Rolleman E and de Jong M (2007) Renal uptake and retention of radiolabeled somatostatin, bombesin, neurotensin, minigastrin and CCK analogues: species and gender differences. Nucl. Med. Biol 34, 633–641, 10.1016/j.nucmedbio.2007.05.002 [PubMed: 17707803]
11. Chen Y, Asico LD, Zheng S, Villar VA, He D, Zhou L et al. (2013) Gastrin and D1 dopamine receptor interact to induce natriuresis and diuresis. Hypertension 62, 927–933, 10.1161/HYPERTENSIONAHA.113.01094 [PubMed: 24019399]

12. Jiang X, Wang W, Ning B, Liu X, Gong J, Gan F et al. (2013) Basal and postprandial serum levels of gastrin in normotensive and hypertensive adults. Clin. Exp. Hypertens 35, 74–78, 10.3109/10641963.2012.690474 [PubMed: 22680232]

13. Martinez-Martinez E, Ibarrola J, Fernandez-Celis A, Calvier L, Leroy C, Cachofeiro V et al. (2018) Galectin-3 pharmacological inhibition attenuates early renal damage in spontaneously hypertensive rats. J. Hypertens 36, 368–376, 10.1097/HJH.0000000000001545 [PubMed: 28858976]

14. Mennuni S, Rubattu S, Pierelli G, Tocci G, Fofi C and Volpe M (2014) Hypertension and kidneys: unraveling complex molecular mechanisms underlying hypertensive renal damage. J. Hum. Hypertens 28, 74–79, 10.1038/jhh.2013.55 [PubMed: 23803592]

15. Huang WY, Li ZG, Rus H, Wang X, Jose PA. and Chen SY (2009) RGC-32 mediates transforming growth factor-beta-induced epithelial-mesenchymal transition in human renal proximal tubular cells. J. Biol. Chem 284, 9426–9432, 10.1074/jbc.M900039200 [PubMed: 19158077]

16. Liao TD, Yang XP, Liu YH., Shesely EG, Cavasin MA, Kuziel WA et al. (2008) Role of inflammation in the development of renal damage and dysfunction in angiotensin II-induced hypertension. Hypertension 52, 256–263, 10.1161/HYPERTENSIONAHA.108.112706 [PubMed: 18541733]

17. Tajbakhsh A, Gheibi Hayat SM, Butler AE and Sahebkar A (2019) Effect of soluble cleavage products of important receptors/ligands on efferocytosis: Their role in inflammatory, autoimmune and cardiovascular disease. Ageing Res. Rev 50, 43–57, 10.1016/j.arr.2019.01.007 [PubMed: 30639340]

18. Zeng Q, Ou L, Wang W and Guo DY (2020) Gastrin, Cholecystokinin, Signaling, and Biological Activities in Cellular Processes. Front. Endocrinol. (Lausanne) 11, 112, 10.3389/fendo.2020.00112 [PubMed: 32210918]

19. Jehle AW, Gardai SJ, Li S, Linsel-Nitschke P, Morimoto K, Janssen WJ et al. (2006) ATP-binding cassette transporter A7 enhances phagocytosis of apoptotic cells and associated ERK signaling in macrophages. J. Cell Biol 174, 547–556, 10.1083/jcb.200601030 [PubMed: 16908670]

20. Sun HJ (2019) Current Opinion for Hypertension in Renal Fibrosis. Adv. Exp. Med. Biol 1165, 37–47, 10.1007/978-981-13-8871-2_3 [PubMed: 31399960]

21. Langhans N, Rindi G, Chiu M, Rehfeld JF, Ardman B, Beinborn M et al. (1997) Abnormal gastric histology and decreased acid production in cholecystokinin-B/gastrin receptor-deficient mice. Gastroenterology 112, 280–286, 10.1016/S0016-5085(97)90000-7 [PubMed: 8978369]

22. Huang XR, Chung AC, Yang F, Yue W, Deng C, Lau CP et al. (2010) Smad3 mediates cardiac inflammation and fibrosis in angiotensin II-induced hypertensive cardiac remodeling. Hypertension 55, 1165–1171, 10.1161/HYPERTENSIONAHA.109.147611 [PubMed: 20231525]

23. Liu GX, Li YQ, Huang XR, Wei L, Chen HY, Shi YJ. et al. (2013) Disruption of Smad7 promotes ANG II-mediated renal inflammation and fibrosis via Sp1-TGF-beta/Smad3-NF.kappaB-dependent mechanisms in mice. PLoS One 8, e53573, 10.1371/journal.pone.0053573 [PubMed: 23301086]

24. Rooman I and Bouwens L (2004) Combined gastrin and epidermal growth factor treatment induces islet regeneration and restores normoglycaemia in C57Bl6/J mice treated with alloxan. Diabetologia 47, 259–265, 10.1007/s00125-003-1287-1 [PubMed: 14666367]

25. Chi HH, Hua KF, Lin YC, Chu CL, Hsieh CY, Hsu YJ. et al. (2017) IL-36 Signaling Facilitates Activation of the NLRP3 Inflammasome and IL-23/IL-17 Axis in Renal Inflammation and Fibrosis. J. Am. Soc. Nephrol 28, 2022–2037, 10.1681/ASN.2016080840 [PubMed: 28179433]

26. Wang S, Tan X, Chen P, Zheng S, Ren H, Cai J et al. (2019) Role of Thioredoxin 1 in Impaired Renal Sodium Excretion of hD 5 R (F173L) Transgenic Mice. J. Am. Heart Assoc 8, e012192, 10.1161/JAHA.119.012192 [PubMed: 30957627]

27. Woost PG, Kolb RJ, Finesilver M, Mackraj I, Imboden H, Coffman TM et al. (2006) Strategy for the development of a matched set of transport-competent, angiotensin receptor-deficient proximal tubule cell lines. In Vitro Cell. Dev. Biol. Anim 42, 189–200, 10.1290/0511076.1 [PubMed: 16948500]

28. Zhu Y, Cui H, Lv J, Liang H, Zheng Y, Wang S et al. (2019) AT1 and AT2 receptors modulate renal tubular cell necroptosis in angiotensin II-infused renal injury mice. Sci. Rep 9, 19450, 10.1038/s41598-019-55550-8 [PubMed: 31857626]
29. Yang X, Yue R, Zhang J, Zhang X, Liu Y, Chen C et al. (2018) Gastrin Protects Against Myocardial Ischemia/Reperfusion Injury via Activation of RISK (Reperfusion Injury Salvage Kinase) and SAFE (Survivor Activating Factor Enhancement) Pathways. J. Am. Heart Assoc 7, e005171 , 10.1161/JAHA.116.005171 [PubMed: 30005556]
30. Gao F, Zuo B, Wang Y, Li S, Yang J and Sun D (2020) Protective function of exosomes from adipose tissue-derived mesenchymal stem cells in acute kidney injury through SIRT1 pathway. Life Sci. 255, 117719, 10.1016/j.lfs.2020.117719 [PubMed: 32428599]
31. Lee SJ, Wang HJ, Kim TH, Choi JS, Kulkarni G, Jackson JD et al. (2018) In Situ Tissue Regeneration of Renal Tissue Induced by Collagen Hydrogel Injection. Stem Cells Transl. Med 7, 241–250, 10.1002/sctm.16-0361 [PubMed: 29380564]
32. Rosen H and Gordon S (1987) Monoclonal antibody to the murine type 3 complement receptor inhibits adhesion of myelomonocytic cells in vitro and inflammatory cell recruitment in vivo. J. Exp. Med 166, 1685–1701, 10.1084/jem.166.6.1685 [PubMed: 2445894]
33. Zhen Y and Shao WH (2019) Experimental Analysis of Apoptotic Thymocyte Engulfment by Macrophages. J. Vis. Exp 147, e59731, 10.3791/59731
34. Paust HJ, Turner JE, Steinmetz OM, Peters A, Heymann F, Holscher C et al. (2009) The IL-23/Th17 axis contributes to renal injury in experimental glomerulonephritis. J. Am. Soc. Nephrol 20, 969–979, 10.1681/ASN.2008050556 [PubMed: 19339380]
35. Luo B, Gan W, Liu Z, Shen Z, Wang J, Shi R et al. (2016) Erythropoeitin Signaling in Macrophages Promotes Dying Cell Clearance and Immune Tolerance. Immunity 44, 287–302, 10.1016/j.immuni.2016.01.002 [PubMed: 26872696]
36. Wang Y, Subramanian M, Yurdagul A Jr, Barbosa-Lorenzi VC, Cai B, de Juan-Sanz J et al. (2017) Mitochondrial Fission Promotes the Continued Clearance of Apoptotic Cells by Macrophages. Cell 171, 331e322–345e322, 10.1016/j.cell.2017.08.041 [PubMed: 28942921]
37. Zhang Y, Wang Y, Zhou D, Zhang LS, Deng FX, Shu S et al. (2019) Angiotensin II deteriorates advanced atherosclerosis by promoting MerTK cleavage and impairing efferocytosis through the AT1R/ROS/p38 MAPK/ADAM17 pathway. Am. J. Physiol. Cell Physiol 317, C776–C787, 10.1152/ajpcell.00145.2019 [PubMed: 31390228]
38. Papadopoulos N, Lennartsson J and Heldin CH (2018) PDGFRbeta translocates to the nucleus and regulates chromatin remodeling via TATA element-modifying factor 1. J. Cell Biol 217, 1701–1717, 10.1083/jcb.201706118 [PubMed: 29545370]
39. You WJ, Fan YF, Xu YH, Wu K and Tan XY (2017) Molecular characterization and functional analysis of PPARalpha promoter in yellow catfish Pelteobagrus fulvidraco. Gene 627, 106–113, 10.1016/j.gene.2017.06.022 [PubMed: 28627437]
40. Kaya-Okur HS, Wu SJ, Codomo CA, Pledger ES, Bryson TD, Henikoff JG et al. (2019) CUT&Tag for efficient epigenomic profiling of small samples and single cells. Nat. Commun 10, 1930 [PubMed: 31036827]
41. Nguyen Ba AN, Pogoutse A, Provart N and Moses AM (2009) NLStradamus: a simple Hidden Markov Model for nuclear localization signal prediction. BMC Bioinformatics 10, 202, 10.1186/1471-2105-10-202 [PubMed: 19563654]
42. Lu Q, Ma Z, Ding Y, Bedarida T, Chen L, Xie Z et al. (2019) Circulating miR-103a-3p contributes to angiotensin II-induced renal inflammation and fibrosis via a SNRK/NF-kappaB/p65 regulatory axis. Nat. Commun 10, 2145, 10.1038/s41467-019-10116-0 [PubMed: 31086184]
43. Martinez-Klimova E, Aparicio-Trejo OE, Tapia E and Pedraza-Chaverri J (2019) Unilateral Ureteral Obstruction as a Model to Investigate Fibrosis-Attenuating Treatments. Biomolecules 9, 141, 10.3390/biom9040141
44. Bijkerk R, Aleksinskaya MA, Duijs J, Veth J, Husen B, Reiche D et al. (2019) Neutral endopeptidase inhibitors blunt kidney fibrosis by reducing myofibroblast formation. Clin. Sci. (Lond.) 133, 239–252, 10.1042/CS20180882 [PubMed: 30617188]
45. Freedman BI and Cohen AH (2016) Hypertension-attributed nephropathy: what's in a name? Nat. Rev. Nephrol 12, 27–36, 10.1038/nrneph.2015.172 [PubMed: 26553514]

46. Xia Y, Entman ML and Wang Y (2013) Critical role of CXCL16 in hypertensive kidney injury and fibrosis. Hypertension 62, 1129–1137, 10.1161/HYPERTENSIONAHA.113.01837 [PubMed: 24060897]
47. Boada-Romero E, Martinez J, Heckmann BL and Green DR (2020) The clearance of dead cells by efferocytosis. Nat. Rev. Mol. Cell Biol 21, 398–414, 10.1038/s41580-020-0232-1 [PubMed: 32251387]
48. Doran AC, Yurdagul A Jr and Tabas I (2020) Efferocytosis in health and disease. Nat. Rev. Immunol 20, 254–267, 10.1038/s41577-019-0240-6 [PubMed: 31822793]
49. Liberale L, Gaul DS, Akhmedov A, Bonetti NR, Nageswaran V, Costantino S et al. (2020) Endothelial SIRT6 blunts stroke size and neurological deficit by preserving blood-brain barrier integrity: a translational study. Eur. Heart J 41, 1575–1587, 10.1093/eurheartj/ehz712 [PubMed: 31603194]
50. Zhong Y, Feng J, Fan Z and Li J (2018) Curcumin increases cholesterol efflux via heme oxygenase1mediated ABCA1 and SRBI expression in macrophages. Mol. Med. Rep 17, 6138–6143 [PubMed: 29436680]
51. Xu P, Gildea JJ, Zhang C, Konkalmatt P, Cuevas S, Bigler Wang D et al. (2020) Stomach gastrin is regulated by sodium via PPAR-alpha and dopamine D1 receptor. J. Mol. Endocrinol 64, 53–65, 10.1530/JME-19-0053 [PubMed: 31794424]
52. Caplin ME, Clarke P, Grimes S, Dhillon AP, Khan K, Savage K et al. (1999) Demonstration of new sites of expression of the CCK-B/gastrin receptor in pancreatic acinar AR42J cells using immunoelectron microscopy. Regul. Pept 84, 81–89, 10.1016/S0167-0115(99)00071-3 [PubMed: 10535412]
53. Yang J, Jose PA. and Zeng C (2017) Gastrointestinal-Renal Axis: Role in the Regulation of Blood Pressure. J. Am. Heart Assoc 6, e005536, 10.1161/JAHA.117.005536 [PubMed: 28264861]
54. Jose PA, Felder RA, Yang Z, Zeng C and Eisner GM (2016) Gastrorenal Axis. Hypertension 67, 1056–1063, 10.1161/HYPERTENSIONAHA.115.06424 [PubMed: 27045027]
55. Jose PA, Yang Z, Zeng C and Felder RA (2016) The importance of the gastrorenal axis in the control of body sodium homeostasis. Exp. Physiol 101, 465–470, 10.1113/EP085286 [PubMed: 26854262]
56. Hallman TM, Peng M, Meade R, Hancock WW, Madaio MP and Gasser DL (2006) The mitochondrial and kidney disease phenotypes of kd/kd mice under germfree conditions. J. Autoimmun 26, 1–6, 10.1016/j.jaut.2005.10.006 [PubMed: 16337774]
57. Vaziri ND, Wong J, Pahl M, Piceno YM, Yuan J, DeSantis TZ et al. (2013) Chronic kidney disease alters intestinal microbial flora. Kidney Int. 83, 308–315, 10.1038/ki.2012.345 [PubMed: 22992469]
58. Wang F, Jiang H, Shi K, Ren Y, Zhang P and Cheng S (2012) Gut bacterial translocation is associated with microinflammation in end-stage renal disease patients. Nephrology (Carlton). 17, 733–738, 10.1111/j.1440-1797.2012.01647.x [PubMed: 22817644]
59. Fujita H, Morii T, Fujishima H, Sato T, Shimizu T, Hosoba M et al. (2014) The protective roles of GLP-1R signaling in diabetic nephropathy: possible mechanism and therapeutic potential. Kidney Int. 85, 579–589, 10.1038/ki.2013.427 [PubMed: 24152968]
60. Park CW, Kim HW, Ko SH, Lim JH, Ryu GR, Chung HW et al. (2007) Long-term treatment of glucagon-like peptide-1 analog exendin-4 ameliorates diabetic nephropathy through improving metabolic anomalies in db/db mice. J. Am. Soc. Nephrol 18, 1227–1238, 10.1681/ASN.2006070778 [PubMed: 17360951]
61. Fujimura K, Wakino S, Minakuchi H, Hasegawa K, Hosoya K, Komatsu M et al. (2014) Ghrelin protects against renal damages induced by angiotensin-II via an antioxidative stress mechanism in mice. PLoS One 9, e94373, 10.1371/journal.pone.0094373 [PubMed: 24747517]
62. Takeda R, Nishimatsu H, Suzuki E, Satonaka H, Nagata D, Oba S et al. (2006) Ghrelin improves renal function in mice with ischemic acute renal failure. J. Am. Soc. Nephrol 17, 113–121, 10.1681/ASN.2004080626 [PubMed: 16306169]
63. Miyamoto S, Shikata K, Miyasaka K, Okada S, Sasaki M, Kodera R et al. (2012) Cholecystokinin plays a novel protective role in diabetic kidney through anti-inflammatory actions on macrophage:

anti-inflammatory effect of cholecystokinin. Diabetes 61, 897–907, 10.2337/db11-0402 [PubMed: 22357963]

64. Jiang X, Chen W, Liu X, Wang Z, Liu Y, Felder RA et al. (2016) The Synergistic Roles of Cholecystokinin B and Dopamine D5 Receptors on the Regulation of Renal Sodium Excretion. PLoS One 11, e0146641, 10.1371/journal.pone.0146641 [PubMed: 26751218]
65. Jiang X, Zhang Y, Yang Y, Yang J, Asico LD, Chen W et al. (2017) Gastrin stimulates renal dopamine production by increasing the renal tubular uptake of l-DOPA. Am. J. Physiol. Endocrinol. Metab 312, E1–E10, 10.1152/ajpendo.00116.2016 [PubMed: 27780818]
66. Liu T, Konkalmatt PR, Yang Y and Jose PA (2016) Gastrin decreases Na+,K+-ATPase activity via a PI 3-kinase- and PKC-dependent pathway in human renal proximal tubule cells. Am. J. Physiol. Endocrinol. Metab 310, E565–571, 10.1152/ajpendo.00360.2015 [PubMed: 26786777]
67. Nath KA (1998) The tubulointerstitium in progressive renal disease. Kidney Int. 54, 992–994, 10.1046/j.1523-1755.1998.00079.x [PubMed: 9734628]
68. Ning WB, Hu GY, Peng ZZ, Wang L, Wang W, Chen JY et al. (2011) Fluorofenidone inhibits Ang II-induced apoptosis of renal tubular cells through blockage of the Fas/FasL pathway. Int. Immunopharmacol 11, 1327–1332, 10.1016/j.intimp.2011.04.016 [PubMed: 21586345]
69. Crowley SD, Frey CW, Gould SK, Griffiths R, Ruiz P, Burchette JL et al. (2008) Stimulation of lymphocyte responses by angiotensin II promotes kidney injury in hypertension. Am. J. Physiol. Renal. Physiol 295, F515–F524, 10.1152/ajprenal.00527.2007 [PubMed: 18495795]
70. Barnawi J, Jersmann H, Haberberger R, Hodge S and Meech R (2017) Reduced DNA methylation of sphingosine-1 phosphate receptor 5 in alveolar macrophages in COPD: A potential link to failed efferocytosis. Respirology 22, 315–321, 10.1111/resp.12949 [PubMed: 27868302]
71. Lacy-Hulbert A, Smith AM, Tissire H, Barry M, Crowley D, Bronson RT et al. (2007) Ulcerative colitis and autoimmunity induced by loss of myeloid alphav integrins. Proc. Natl. Acad. Sci. U. S. A 104, 15823–15828, 10.1073/pnas.0707421104 [PubMed: 17895374]
72. Colonna L, Lood C and Elkon KB (2014) Beyond apoptosis in lupus. Curr. Opin. Rheumatol 26, 459–466, 10.1097/BOR.0000000000000083 [PubMed: 25036095]
73. Harada M, Kamijo Y, Nakajima T, Hashimoto K, Yamada Y, Shimojo H et al. (2016) Peroxisome proliferator-activated receptor alpha-dependent renoprotection of murine kidney by irbesartan. Clin. Sci. (Lond.) 130, 1969–1981, 10.1042/CS20160343 [PubMed: 27496805]
74. Zhou Y, Kong X, Zhao P, Yang H, Chen L, Miao J et al. (2011) Peroxisome proliferator-activated receptor-alpha is renoprotective in doxorubicin-induced glomerular injury. Kidney Int. 79, 1302–1311, 10.1038/ki.2011.17 [PubMed: 21368746]
75. Boor P, Celec P, Martin IV, Villa L, Hodosy J, Klenovicsova K et al. (2011) The peroxisome proliferator-activated receptor-alpha agonist, BAY PP1, attenuates renal fibrosis in rats. Kidney Int. 80, 1182–1197, 10.1038/ki.2011.254 [PubMed: 21814170]
76. Cheng R, Ding L, He X, Takahashi Y and Ma JX (2016) Interaction of PPARalpha With the Canonic Wnt Pathway in the Regulation of Renal Fibrosis. Diabetes 65, 3730–3743, 10.2337/db16-0426 [PubMed: 27543085]
77. Jao TM, Nangaku M, Wu CH, Sugahara M, Saito H, Maekawa H et al. (2019) ATF6alpha downregulation of PPARalpha promotes lipotoxicity-induced tubulointerstitial fibrosis. Kidney Int. 95, 577–589, 10.1016/j.kint.2018.09.023 [PubMed: 30639234]
78. Lyu H, Li X, Wu Q and Hao L (2019) Overexpression of microRNA-21 mediates Ang II-induced renal fibrosis by activating the TGF-beta1/Smad3 pathway via suppressing PPARalpha. J. Pharmacol. Sci 141, 70–78, 10.1016/j.jphs.2019.09.007 [PubMed: 31611175]
79. Nagothu KK, Bhatt R, Kaushal GP and Portilla D (2005) Fibrate prevents cisplatin-induced proximal tubule cell death. Kidney Int. 68, 2680–2693, 10.1111/j.1523-1755.2005.00739.x [PubMed: 16316343]
80. Katschinski M, Dahmen G, Reinshagen M, Beglinger C, Koop H, Nustede R et al. (1992) Cephalic stimulation of gastrointestinal secretory and motor responses in humans. Gastroenterology 103, 383–391, 10.1016/0016-5085(92)90825-J [PubMed: 1634057]
81. Begg DP and Woods SC (2013) The endocrinology of food intake. Nat. Rev. Endocrinol 9, 584–597, 10.1038/nrendo.2013.136 [PubMed: 23877425]

82. Hancock ML, Meyer RC, Mistry M, Khetani RS, Wagschal A, Shin T et al. (2019) Insulin Receptor Associates with Promoters Genome-wide and Regulates Gene Expression. Cell 177, 722e722–736e722, 10.1016/j.cell.2019.02.030 [PubMed: 30955890]

83. Lin SY, Makino K, Xia W, Matin A, Wen Y, Kwong KY et al. (2001) Nuclear localization of EGF receptor and its potential new role as a transcription factor. Nat. Cell Biol 3, 802–808, 10.1038/ncb0901-802 [PubMed: 11533659]

84. Kesten D, Horovitz-Fried M, Brutman-Barazani T and Sampson SR (2018) Insulin-induced translocation of IR to the nucleus in insulin responsive cells requires a nuclear translocation sequence. Biochim. Biophys Acta. Mol. Cell Res 1865, 551–559, 10.1016/j.bbamcr.2018.01.004 [PubMed: 29317261]

85. Hsu SC and Hung MC (2007) Characterization of a novel tripartite nuclear localization sequence in the EGFR family. J. Biol. Chem 282, 10432–10440, 10.1074/jbc.M610014200 [PubMed: 17283074]

Clinical perspectives

- Emerging data demonstrate that gastrin and its receptor CCKBR are linked to hypertensive nephropathy.
- We demonstrate for the first time that the infusion of gastrin decreases renal tubule cell apoptosis, increases macrophage efferocytosis, and prevents the development and progression of HN in a mouse model. We demonstrate for the first time that gastrin induces CCKBR translocation from the cytosol to the nucleus, binding to the PPAR-a promoter region, and increasing PPAR-a gene transcription ability.
- Gastrin and CCKBR might be potential target in HN therapy.

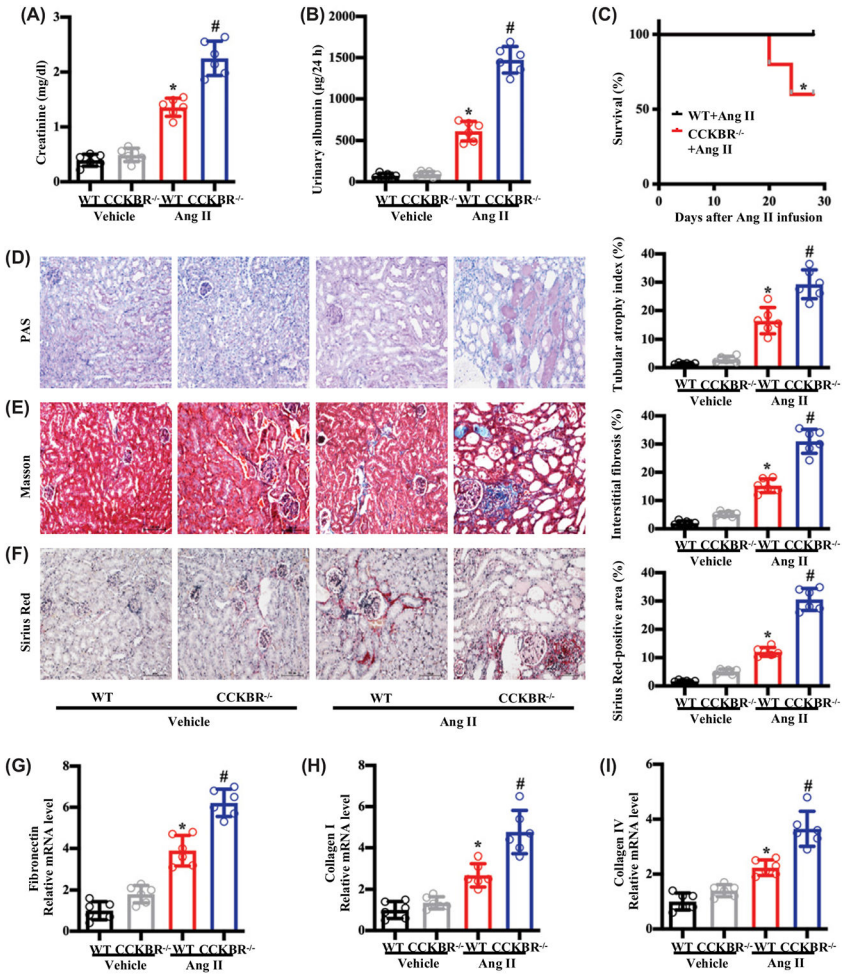

Figure 1. CCKBR deficiency aggravates Ang II-induced renal injury and fibrosis

WT (CCKBR$^{+/+}$) and CCKBR$^{-/-}$ mice were infused subcutaneously, via osmotic minipump, with saline vehicle (control, 2.64 μl/d) or Ang II (1.44 mg/kg body weight/d) for 28 d. The samples were collected at the end of 28 d. (**A** and **B**) Serum creatinine (A) and urinary albumin (B) were quantified. n=6; *P<0.05 vs. WT+Vehicle treatment; $^{\#}P$<0.05 vs. WT+Ang II treatment. (**C**) Survival analysis of WT and CCKBR$^{-/-}$ mice infused with Ang II (1.44 mg/kg body weight/d) for 28 d. n=10; *P<0.05 vs. WT+Ang II treatment. (**D**) Representative images of PAS staining and quantitative analysis of renal tubular injury. n=6; *P<0.05 vs. WT+Vehicle treatment mice; $^{\#}P$<0.05 vs. WT+Ang II treatment. (**E**) Representative images of Masson's trichrome staining and quantitative analysis of renal interstitial fibrosis. n=6; *P<0.05 vs. WT+Vehicle treatment; $^{\#}P$<0.05 vs. WT+Ang II treated. (**F**) Representative images of Sirius Red staining and quantitative analysis of Sirius Red-positive areas showing the renal collagen deposition. n=6; *P<0.05 vs. WT+Vehicle treatment mice; *$^{\#}P$<0.05 vs. WT+Ang II treatment mice. (**G–I**) Fibrosis-related mRNA levels in the kidney: fibronectin (G); collagen I (H); and collagen IV (I). n=6; *P<0.05 vs. WT+Vehicle treatment; $^{\#}P$<0.05 vs. WT+Ang II treatment.

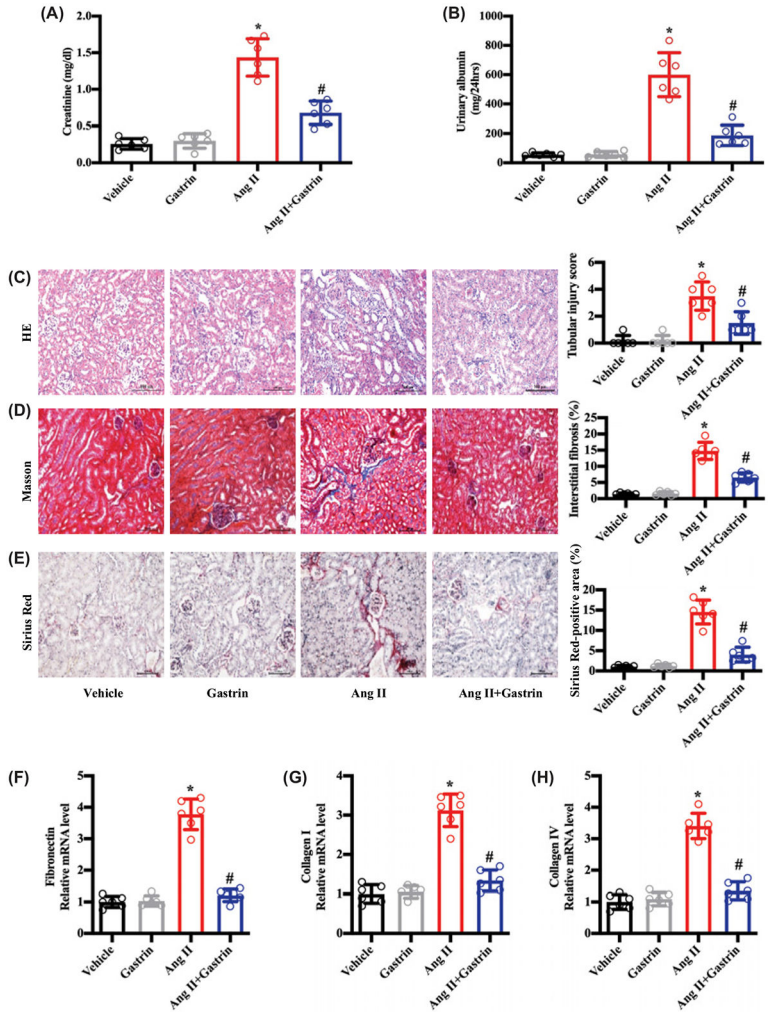

Figure 2. Gastrin, independent of blood pressure, attenuates Ang II-induced renal injury

WT (CCKBR$^{+/+}$) mice were infused subcutaneously, via an osmotic minipump, with saline vehicle (control, 2.64 μl/d), Ang II (1.44 mg/kg body weight/d), and/or gastrin (120 μg/kg body weight/d) for 28 d. The samples were collected at the end of 28 d. (**A** and **B**) Serum creatinine (A) and urinary albumin (B) were quantified. n=6; *P<0.05 vs. Vehicle treatment; $^{\#}P$<0.05 vs. Ang II treatment. (**C**) Representative images of H&E staining and quantitative analysis of renal tubular injury. n=6; *P<0.05 vs. Vehicle treatment; $^{\#}P$<0.05 vs. Ang II treatment. (**D**) Representative images of Masson's trichrome staining and quantitative analysis of renal interstitial fibrosis. **n**=6; ***P**<0.05 vs. Vehicle treatment; $^{\#}P$<0.05 vs. Ang II treatment. (**E**) Representative images of Sirius Red staining and quantitative analysis of Sirius Red-positive areas showing the renal collagen deposition. n=6; *P<0.05 vs. Vehicle treatment; $^{\#}P$<0.05 vs. Ang II treatment. (**F–H**) Fibrosis-related mRNA levels in the kidney: fibronectin (F); collagen I (G); and collagen IV (H). n=6; *P<0.05 vs. Vehicle treatment; $^{\#}P$<0.05 vs. Ang II treatment.

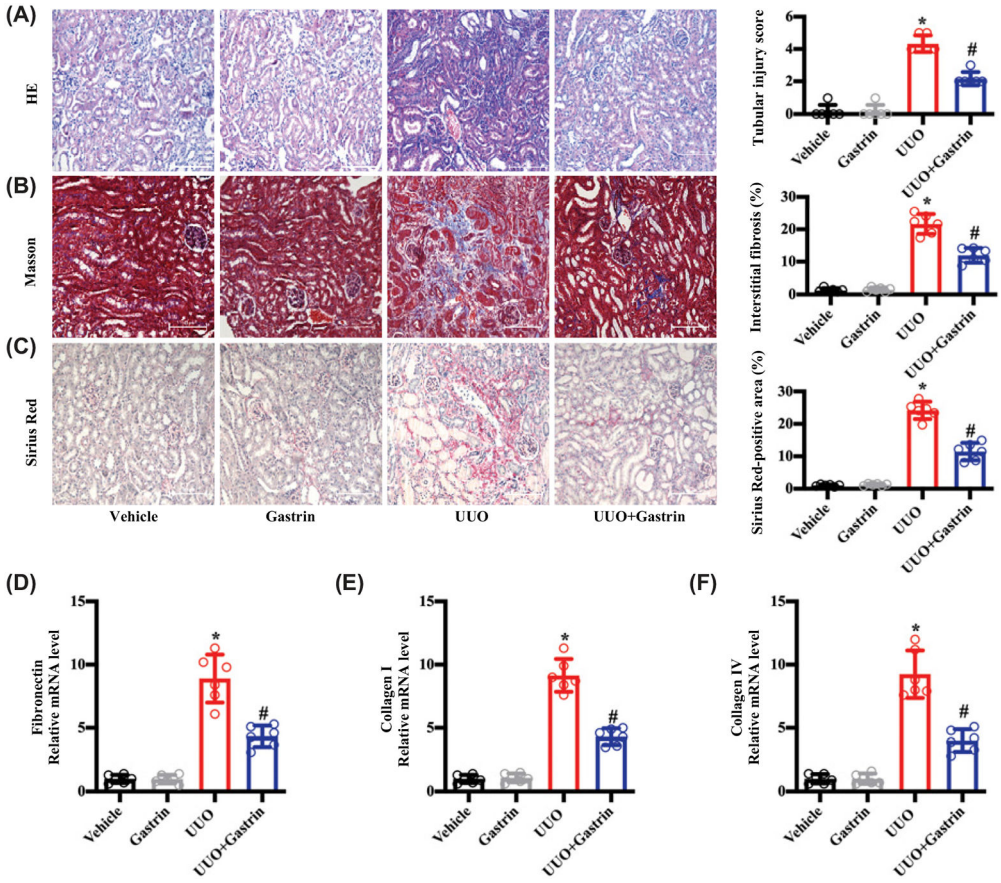

Figure 3. Gastrin attenuates renal fibrosis caused by UUO

Mice with UUO or sham-operated mice were infused subcutaneously, via an osmotic minipump with saline vehicle (control, 2.64 μl/d) or gastrin (120 μg/kg body weight /d x 7 d). The samples were collected at the end of 7 d. (**A**) Representative images of H&E staining and quantitative analysis of renal tubular injury. n=6; *P<0.05 vs. Vehicle treatment; $^{\#}P$<0.05 vs. Ang II treatment. (**B**) Representative images of Masson's trichrome staining and quantitative analysis of renal interstitial fibrosis. n=6; *P<0.05 vs. Vehicle treatment; $^{\#}P$<0.05 vs. Ang II treatment. (**C**) Representative images of Sirius Red staining and quantitative analysis of Sirius Red-positive areas showing renal collagen deposition. n=6; *P<0.05 vs. Vehicle treatment; $^{\#}P$<0.05 vs. Ang II treatment. (**D–F**) Fibrosis-related mRNA levels in the kidney: fibronectin (D); collagen I (E); and collagen IV (F). n=6; *P<0.05 vs. Vehicle treatment; $^{\#}P$<0.05 vs. Ang II treatment.

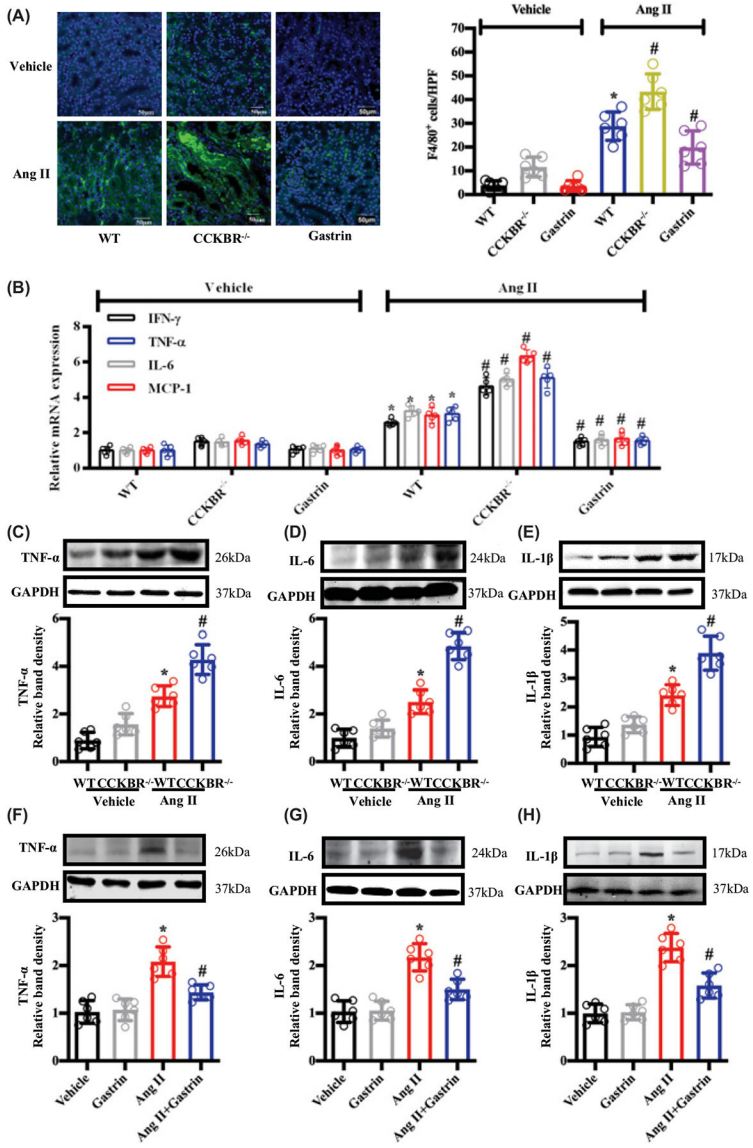

Figure 4. The effects of CCKBR deficiency and gastrin treatment in Ang II-induced renal inflammation

WT (CCKBR$^{+/+}$) and CCKBR$^{-/-}$ mice were subcutaneously infused, via osmotic minipump with saline vehicle (control, 2.64 μl/d), Ang II (1.44 mg/kg body weight/d), and/or gastrin (120 μg/kg body weight/d) for 28 d. The samples were collected at the end of 28 d. (**A**) Immunofluorescence microscopy of F4/80 (macrophage marker) in the kidney. The left images are representative images of renal F4/80 staining. The graph, on the right, is the quantification of F4/80^{+} cells per high power field (HPF). n=6; *P<0.05 vs. WT+Vehicle treatment; $^{\#}P$<0.05 vs. WT+Ang II treatment. (**B**) Proinflammatory cytokines mRNA expression in the kidneys of WT (CCKBR$^{+/+}$) and CCKBR$^{-/-}$ mice treated with saline vehicle (control) or Ang II. WT mice were also treated with vehicle+gastrin or Ang II+gastrin. n=5; *P<0.05 vs. WT+Vehicle treatment; $^{\#}P$<0.05 vs. WT+Ang II treatment. (**C–E**) Western blots and relative band densities of protein levels of inflammation markers in the kidney in WT and CCKBR$^{-/-}$ mice treated with vehicle or Ang II: TNF-α (C); IL-6 (D); and

IL-1β (E). n=6; *P<0.05 vs. WT+Vehicle treatment; $^{\#}P$<0.05 vs. WT+Ang II treatment. (**F–H**) Western blots and relative band densities of the protein levels of inflammation markers in the kidney of WT mice treated with vehicle, gastrin, Ang II, or gastrin+Ang II: TNF-α (F); IL-6 (G); and IL-1β (H) proteins. n=6; *P<0.05 vs. Vehicle treatment; $^{\#}P$<0.05 vs. Ang II treatment.

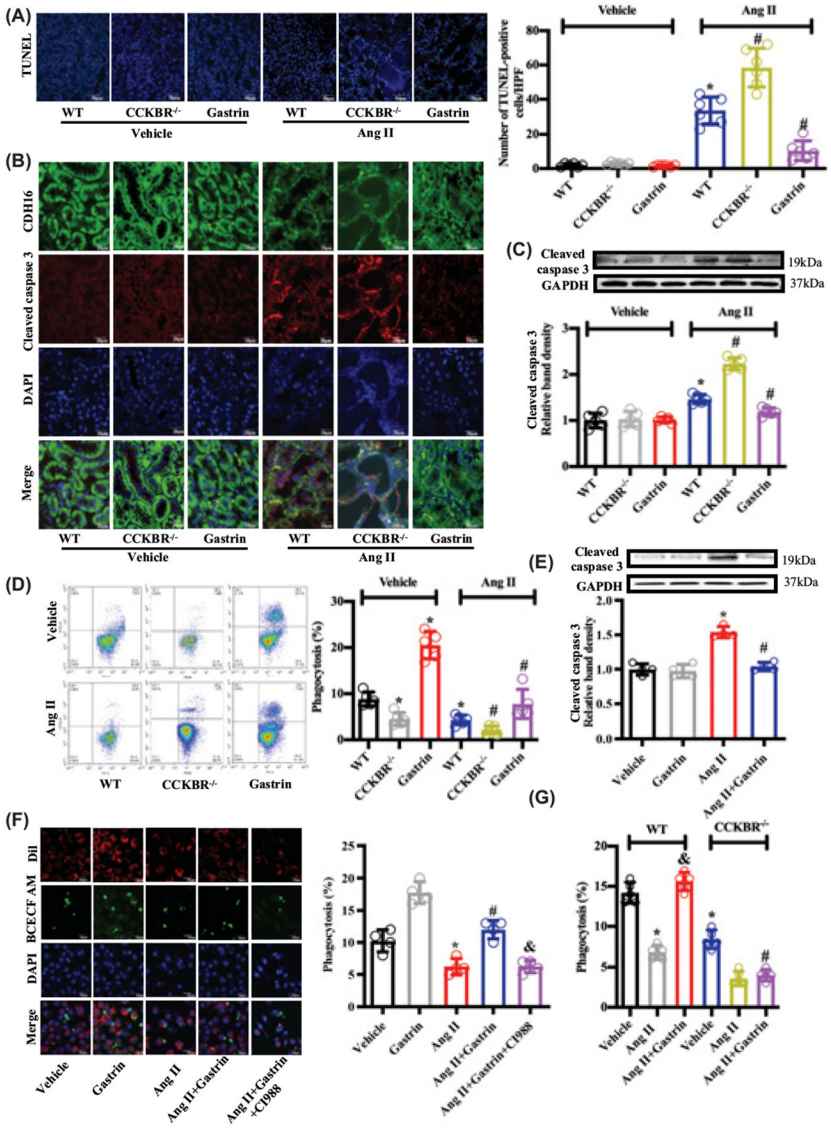

Figure 5. The effects of CCKBR deficiency and gastrin treatment on renal tubule cell apoptosis and macrophage efferocytosis

WT (CCKBR$^{+/+}$) and CCKBR$^{-/-}$ mice were subcutaneously infused, via osmotic minipump, with saline vehicle (control, 2.64 μl/d), Ang II (1.44 mg/kg body weight/d) and/or gastrin (120 μg/kg body weight/d) for 28 d. The kidney samples were collected at the end of 28 d. (**A**) TUNEL staining (green) in the kidney from the different groups (left panel). TUNEL-positive nuclei (the right panel) are increased by Ang II to a greater extent in CCKBR$^{-/-}$ than WT mice. Gastrin decreased the number of apoptotic renal cells in Ang II-treated WT mice. n=6; *P<0.05 vs. WT+Vehicle treatment; $^{\#}P$<0.05 vs. WT+Ang II treatment. (**B**) Representative fluorescent images of CDH16 (cadherin-16, marker of renal tubule cell), cleaved caspase 3 (marker of apoptosis), and DAPI in kidney, showing that CCKBR deficiency increased, while gastrin decreased the expression of cleaved caspase 3 induced by Ang II in HN mice; n=5. (**C**) Western blots and relative band densities of cleaved caspase 3 in the kidney of WT and CCKBR$^{-/-}$ mice; n=5; *P<0.05 vs.

WT+Vehicle treatment; $^{\#}P<0.05$ vs. WT+Ang II treatment. (**D**) WT or CCKBR$^{-/-}$ mice were subcutaneously infused, via osmotic minipump, with saline vehicle (control, 2.64 μl/d), Ang II (1.44 mg/kg body weight/d) and/or gastrin (120 μg/kg body weight/d) for 28 d. Then, peritoneal macrophages were harvested by peritoneal lavage. The percentage of peritoneal macrophages (F4/80^{+}CD11b^{+}) containing BCECF AM-related fluorescence was quantified by fluorescence-activated cell sorting 1 h after the intraperitoneal injection of BCECF AM-labeled apoptotic cells (left image). Then, the phagocytosis index was calculated (right graph); $n=5$; $^{*}P<0.05$ vs. WT+Vehicle treatment; $^{\#}P<0.05$ vs. WT+Ang II treatment. (**E**) Western blots and relative band densities of cleaved caspase 3 (marker of apoptosis) in RPT cells treated with saline vehicle (control, 25 μl), gastrin (10^{-7} mol/l), and/or Ang II (10^{-8} mol/l) for 24 h; $n=4$; $^{*}P<0.05$ vs. Vehicle treatment; $^{\#}P<0.05$ vs. Ang II treatment. (**F**) Representative fluorescent images show the engulfing (efferocytosis) of apoptotic Jurkat cells (BCECF AM) by RAW264.7 cells (Dil-stained) with saline vehicle (control, 20 μl), gastrin (10^{-7} mol/l), Ang II (10^{-8} mol/l), and/or CI988 (10^{-7} mol/L) treatment for 24 h (left image). Efferocytosis is determined by bound macrophages or ingestion of at least one Jurkat cell. The phagocytic index is based on the fluorescent images (right graph). $n=4$; $^{*}P<0.05$ vs. Vehicle treatment; $^{\#}P<0.05$ vs. Ang II treatment; $^{\&}P<0.05$ vs. Ang II+Gastrin treatment. (**G**) Phagocytic index of primary cultures of peritoneal macrophages from WT and CCKBR$^{-/-}$ mice treated with saline vehicle (control, 20 μl), Ang II (10^{-8} mol/l) alone, or gastrin (10^{-7} mol/l); n=5; $^{*}P<0.05$ vs. WT+Vehicle treatment; $^{\#}P<0.05$ vs. WT+Ang II+Gastrin treatment; $^{\&}P<0.05$ vs. WT+Ang II treatment.

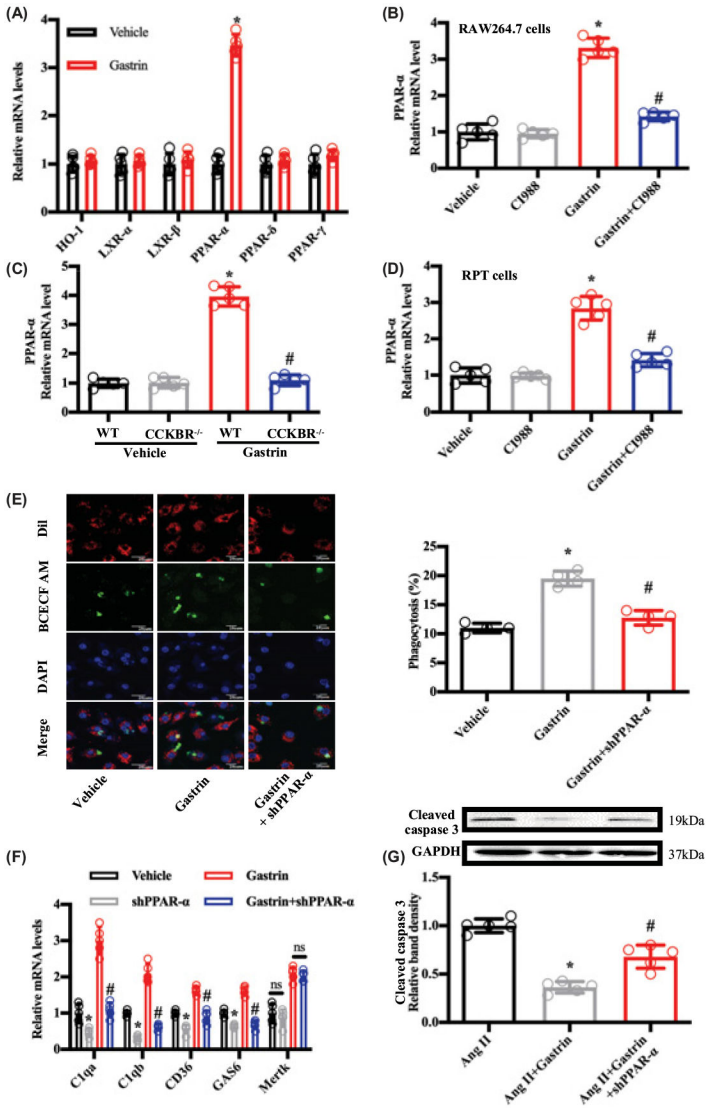

Figure 6. Gastrin reduces Ang II-induced RPT cell apoptosis and enhances the efferocytosis of macrophages through PPAR-*α*

(**A**) RAW264.7 cells were incubated with saline vehicle (control, 25 μl) or gastrin (10^{-7} mol/l) for 24 h prior to measuring the mRNA expression of phagocytosis-associated genes. n=5; *P<0.05 vs. Vehicle treatment. (**B**) RAW264.7 cells were incubated with saline vehicle (control, 25 μl), CI988 (10^{-7} mol/l), gastrin (10^{-7} mol/l) or gastrin (10^{-7} mol/l) + CI988 (10^{-7} mol/l) for 24 h, prior to measuring PPAR-α mRNA. n=5; *P<0.05 vs. others; #P<0.05 vs. Gastrin treatment. (**C**) Primary cultures of peritoneal macrophages from WT and CCKBR$^{-/-}$ mice were incubated with saline vehicle (control, 25 μl) or gastrin (10^{-7} mol/l) for 24 h, prior to measuring PPAR-α mRNA. n=5; *P<0.05 vs. WT+Vehicle treatment; #P<0.05 vs. WT+Gastrin treatment. (D) RPT cells were incubated with saline vehicle (control, 25 μl), CI988 (10^{-7} mol/l), gastrin (10^{-7} mol/l), or gastrin (10^{-7} mol/l) +CI988 (10^{-7} mol/l) for 24 h, prior to measuring PPAR-α mRNA. n=5; *P<0.05 vs. others; #P<0.05 vs. Gastrin treatment. (**E**) Representative fluorescent images showing engulfment of apoptotic Jurkat cells (BCECF AM) by RAW264.7 cells (Dil) (left panel). RAW264.7

cells were infected with lentivirus expressing PPAR-α shRNA or control shRNA, and then treated with saline vehicle (control, 20 μl) or gastrin (10^{-7} mol/l) for 24 h prior to measuring efferocytosis (right graph). n=4; *P<0.05 vs. Vehicle treatment; $^{\#}P$<0.05 vs. Gastrin treatment. (F) RAW264.7 cells were infected with lenti-shPPAR-α or lentiviral particles vehicle (scramble shRNA transfected with lentiviral particles used as vehicle control) for 72 h, prior to gastrin (10^{-7} mol/l) treatment for 24 h. Efferocytosis-related mRNA was quantified by qRT-PCR. n=5; *P<0.05 vs. Vehicle treatment; $^{\#}P$<0.05 vs. Gastrin treatment. (**G**) Western blots of cleaved caspase 3 (marker of apoptosis) in RPT cells. RPT cells were infected with lenti-shPPAR-α or lentiviral particles vehicle (scramble shRNA transfected with lentiviral particles used as vehicle control), and then treated with Ang II (10^{-8} mol/l), alone or with gastrin (10^{-7} mol/l) for 24 h prior to Western blotting. n=5; *P<0.05 vs. Ang II treatment; $^{\#}P$<0.05 vs. Ang II+Gastrin treatment.

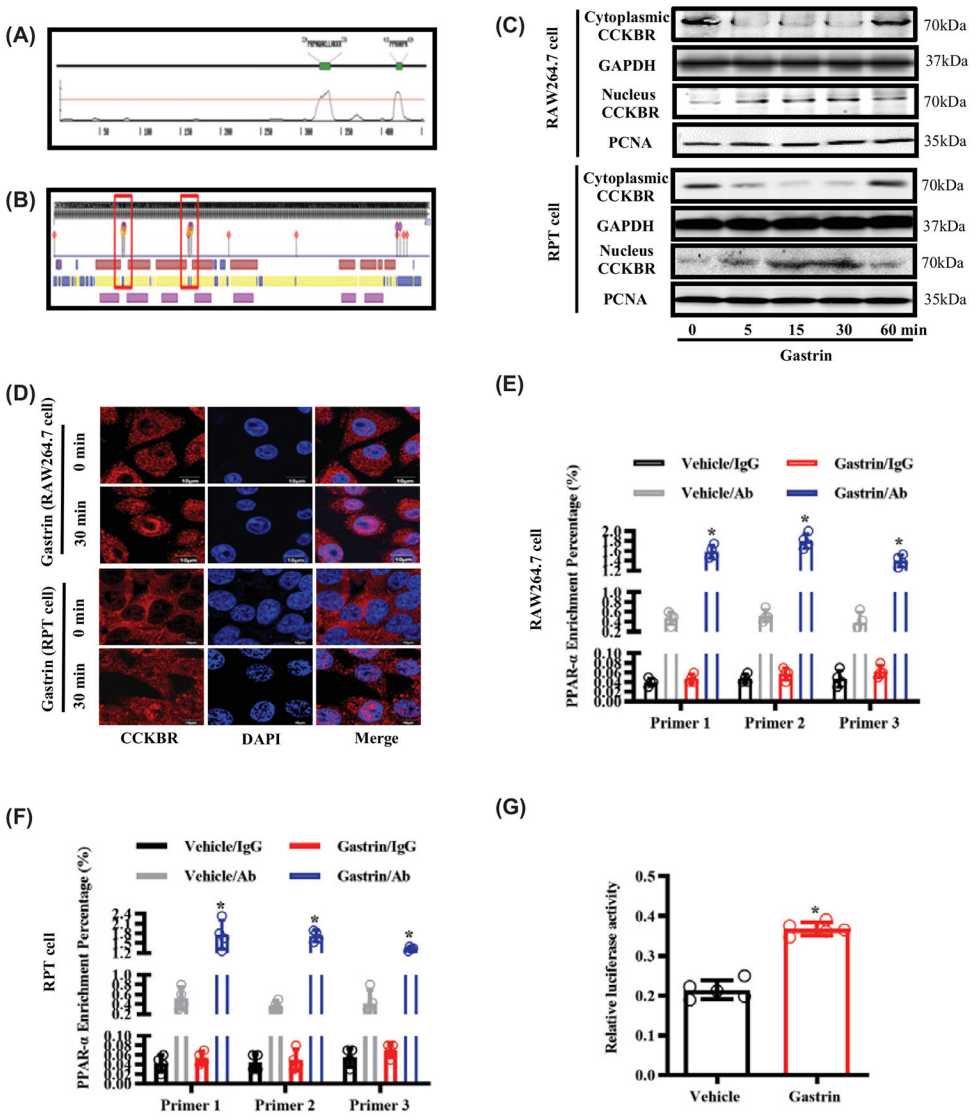

Figure 7. CCKBR translocates into the nucleus and facilitates the activation of PPAR-*α* after gastrin treatment

(**A**) Bioinformatics analysis of NLS motifs in CCKBR showing the location and composition of NLS motifs. (**B**) Bioinformatics analysis of DNA binding domains in CCKBR, and the locations of DNA binding domains (red frame). (**C**) RAW264.7 cells and RPT cells were treated with gastrin (10^{-7} mol/l) for 0, 5, 15, 30, and 60 min, prior to Western blot analyses of nuclear and cytoplasmic distribution of CCKBR. PCNA is a gene marker; n=4. (**D**) RAW264.7 cells and RPT cells were treated with gastrin (10^{-7} mol/l) for 0 and 30 min prior to the immunofluorescence analyses of nuclear and cytoplasmic distribution of CCKBR. CCKBR was stained with CCKBR antibody (red); chromatin was stained with DAPI (blue); n=4. (**E**) RAW264.7 cells were treated with saline vehicle (control, 25 μl) or gastrin (10^{-7} mol/l) for 30 min, prior to quantifying the percent enrichment of CCKBR at the PPAR-*α* gene, using Cut&tag-qPCR; n=4; *P<0.05 vs. Vehicle treatment with CCKBR antibody (Ab). (**F**) RPT cells were treated with saline vehicle (control, 25 μl) or gastrin (10^{-7} mol/l) for 30 min, prior to quantifying the percent

enrichment of CCKBR at the PPAR-α gene. using Cut&tag-qPCR; n=4; *P<0.05 vs. Vehicle treatment with CCKBR antibody (Ab). (**G**) HEK293 cells, co-transfected with CCKBR-FLAG, PPAR-α promoter-pGL3, and pRL-TK, were treated with saline vehicle (control, 10 μl) or gastrin (10^{-7} mol/l) for 24 h, prior to measuring PPAR-α promoter luciferase reporter activity; n=5; *P<0.05 vs. Vehicle treatment.